# The Convex-Concave Ambiguity in Perspective Shape from Shading

Michael Breuß[1], Ashkan Mansouri Yarahmadi[1] and Douglas Cunningham[2]

*Abstract*— Shape from Shading (SFS) is a classic problem in computer vision. In recent years many perspective SFS models have been studied that yield useful SFS approaches when a photographed object is close to the camera. However, while the ambiguities inherent to the classical, orthographic SFS models are well-understood, there has been no discussion of possible ambiguities in perspective SFS models. In this paper we deal with the latter issue. Therefore we adopt a typical perspective SFS setting. We show how to transform the corresponding image irradiance equation into the format of the classical orthographic setting by employing spherical coordinates. In the latter setting we construct a convex-concave ambiguity for perspective SFS. It is to our knowledge the first time in the literature that this type of ambiguity is constructed and verified for a perspective SFS model.

## I. INTRODUCTION

*Shape from Shading (SFS)* is a fundamental problem in computer vision [6]. Given a single greyscale input image, the SFS process makes use of the variation of grey values appearing by light reflectance at an objects' surface to reconstruct the 3D shape. In order to avoid ill-posedness in the reconstruction process as much as possible, especially modeling assumptions on illumination and light reflectance in a scene are employed in SFS.

The classic SFS model assumes the camera to perform an orthographic projection, that light falls on the scene of interest in parallel rays from infinity and that photographed objects have a Lambertian surface yielding the light reflectance, cf. [6], [7]. Within the last years the setting of perspective camera projection has received much attention in SFS, which we consider here as the *perspective shape-from-shading (PSFS)* models. For some milestones in the development of PSFS, let us mention here Lee and Kuo [10] who formulate an image irradiance equation with Lambertian surfaces and a nearby light source, including yet simplifications such as image formation over triangular surface patches and a linear approximation of the reflectance map. There are several groups who worked on more general models formulated explicitly by *partial differential equations (PDEs)* [3], [12], [16]. These models also feature Lambertian surface reflectance and parallel lighting from infinity. Furthermore, Prados and Faugeras considered a point light source in finite range of the photographed scene – more specifically, putting it at the center of projection, being roughly equivalent to modeling a camera with flashlight – and introduced a light

attenuation factor. The latter enables some degree of well-posedness [1], [13], [14] but also makes the model itself considerably more complicated.

The arguably most studied SFS model in the SFS literature is the classic SFS described by Horn [5], see also [17]. As a particular feature, it involves the *convex-concave ambiguity* [7]. This means, given an input image of an object, the classic SFS model itself cannot distinguish between convex and concave versions of the objects' surface, e.g. a photographed mound (convex) seen from above and with lighting from above could as well be a photographed cavity (concave) of the analogous form. Let us note that the convex-concave ambiguity is of interest not only in computer vision, but also in the context of understanding models of human perception; for example, if the silhouette edge information specifies a convex shape, cf. [9], then human perceivers will have a strong bias towards seeing the surface as convex regardless of other shading factors such as specular highlights [11].

**Our Contribution.** In this paper, we show for the first time in the literature that also PSFS models may exhibit the convex-concave ambiguity. The model set-up we explore incorporates in addition to the perspective camera projection and Lambertian surface reflection that the light source is at the projection center. This choice coincides with the light source position employed by Prados and Faugeras. Similarly to the proceeding in [4], [8], where different models as here were considered, we propose to reformulate the arising PDE in a *spherical coordinate system*. We show that the reformulated PDE is in spherical coordinates of *exactly the same form* as the classic PDE of orthographic SFS from Horn. By exploring then the known mechanisms of the convex-concave ambiguity for classic SFS, we construct the corresponding ambiguity for PSFS. We show this construction here in detail for input signals, but it is evident that the proceeding can easily be extended in a straightforward way to images.

## II. SHAPE FROM SHADING SET-UP

In the next paragraphs we briefly elaborate on the orthographic as well as the perspective camera projections and SFS models.

### A. Orthographic Shape from Shading

For the classic orthographic SFS model, in addition to the projection itself the position of light source and the surface normal vectors used in the Lambertian reflectance formula are the main construction elements. Let us review them one by one, recalling thereby the setting described in more detail in [6], [7].

[1]Brandenburg Technical University, Institute of Mathematics, Platz der Deutschen Einheit 1, 03046 Cottbus, Germany `{breuss,ashkan.mansouriyarahmadi}@b-tu.de`
[2]Brandenburg Technical University, Institute of Computer Science, Konrad-Wachsmann-Allee 5, 03046 Cottbus, Germany `douglas.cunningham@b-tu.de`

**Coordinate system.** Our choice is identical to the classic setting of a right handed coordinate system shown in Figure 1. The motivation behind this is to have the outward normals to the surface $z = f(X,Y)$ pointing always to the positive direction of the $z$-axis.

**Lighting.** The light source is assumed to be far away from the scene and placed at the positive side of the z axis, uniformly illuminating the surface as parallel beams coming from infinity. In this way, the outward normals of the surface always point to the light source. To model this, we employ the light vector $\omega = (\omega_1, \omega_2, \omega_3)^\top$ as the representative of the existing light in scene and consider its length to be unit. About the direction of $\omega$, it is convenient to direct it from the surface to the light source, since in this case the outward normal to the surface and the light vector both point to the positive side of the $z$-axis and the incident angle $\theta$ among them is of interest.

**Surface normal vectors.** The normal vector $\mathbf{n} = (-p, -q, 1)^\top$ describes the surface geometry. The surface normals always point to the positive side of the $z$-axis. Here, $p$ and $q$ are the rate of change of surface $f$ in $x$ and $y$ directions, respectively.

**Lambertian reflectance.** The irradiance of a Lambertian surface depends only on the angle between the normal $\mathbf{n}$ at a surface point with the light vector $\omega$ reaching to that point. Thus a Lambertian surface looks identical from any point it is observed. This is formalized by Lambert's cosine law

$$I(x,y) = \rho(x,y)(\omega \cdot \mathbf{n}(x,y)) \tag{1}$$

where $\rho$ represents the albedo of the Lambertian surface, which we set for simplicity always equal to one in this paper.

This setting allows to formulate an *eikonal equation* as the constituting equation of classical, orthographic SFS:

$$\|\nabla u(x,y)\| = \sqrt{\frac{1}{I(x,y)^2} - 1} \tag{2}$$

Here, $I(x,y)$ is the image irradiance found at the pixel with coordinates $(x,y)$ in the input image.

Let us note that in the constituting equation (2), the depth of the unknown surface $u(x,y)$ is described in terms of first-order derivatives within the nabla operator. Therefore one may add an arbitrary constant $\alpha$ to the depth, obtaining $u(x,y) + \alpha$, and obtain the same PDE as in (2). Consequently, the PDE (2) describes the *shape* of an object up to a free *additive* parameter, but not the actual depth in a scene.

*B. Perspective Shape from Shading*

In simplest form the perspective projection could be performed by a *pinhole camera*, see Figure 2. Let us note that we specify the world coordinate system by capital letters, while we write small letters for coordinates in the image coordinate system, given in the image plane. This distinction is of some importance in the perspective setting, and in below paragraphs we give more details.
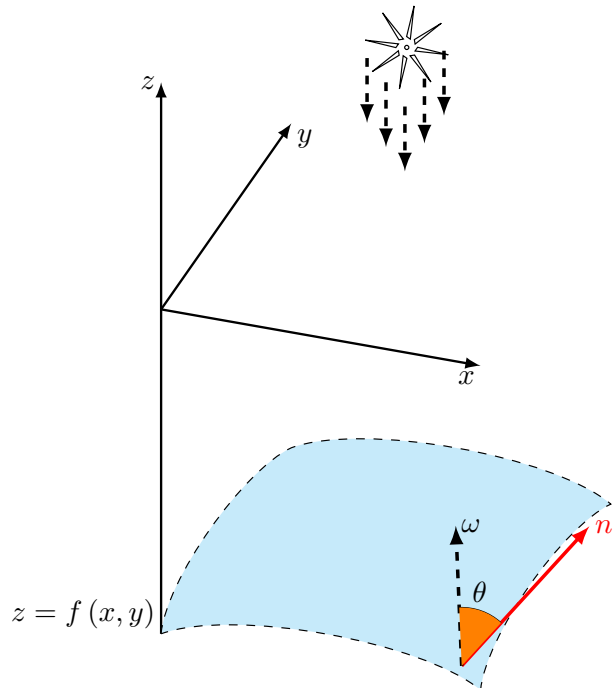


Fig. 1: An orthographic setup with a surface $z = f(x,y)$ to be located at the negative side of the $z$ axis. The source of light $\omega$ is assumed to be located at infinity illuminating the surface as parallel beams in direction of $z$-axis, as seen from the surface. In such a setup, every object point $(x,y,z)$ is projected to the image plane $(x,y)$. Let us note that world coordinates $(X,Y)$ are here identical to image coordinates $(x,y)$, so we do not distinguish these coordinate systems explicitly in the orthographic setting.

**World coordinate system.** To describe any point in a scene, three axis of $X$, $Y$ and $Z$ are used. They form a right-handed coordinate system as shown in Figure 2.

**Image plane.** It is spanned by two axis, featuring $x$ and $y$ as coordinates, as depicted in Figure 2 and its origin $c$ is called principal point. The image plane is located at the distance $Z = f$ from the origin $C$ of the world coordinate system. Here $f$ is the focal length of the pinhole camera.

It is important to note that one may describe the perspective projection via

$$\Delta: \begin{pmatrix} X \\ Y \\ Z \end{pmatrix} \in \mathbb{R}^3 \mapsto \underbrace{\begin{pmatrix} fX/Z \\ fY/Z \end{pmatrix}}_{(x,y)^T} \in \mathbb{R}^2 \tag{3}$$

where $f$ is again the focal length.

Let us note here that all points along the lines of projection – i.e. with the same ratio $X/Z$ and $Y/Z$, respectively, as exemplified in dashed red in Figure 2 – are mapped to the same point in the image plane. Therefore, even without making it explicit, it is evident that in our setting of perspective SFS
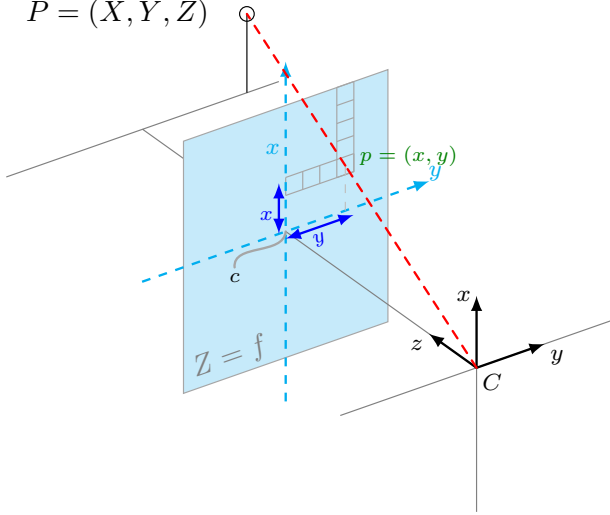
Fig. 2: A schematic view of perspective projection with an adopted pinhole camera. Here we distinguish between world coordinates and image coordinates.

there is a free *multiplicative* parameter that allows to scale the world coordinates. It is not an additive one as in the orthographic setting.

## III. PERSPECTIVE SFS AS EIKONAL EQUATION

We proceed by parametrizing a surface of interest within the spherical coordinate system. In the next paragraphs we derive in detail the needed components, namely the parametrized surface, the gradient, the basis vectors, the normal vectors and the light vector all in the spherical coordinate system. Having these components in hand, we could further derive the constituting equation of PSFS in terms of an eikonal equation.

### A. Surface parametrization

We consider the surface point $(X, Y, Z)$ in world coordinate system and present it as a vector $\mathbf{u}$:

$$\mathbf{u} := \begin{pmatrix} X \\ Y \\ Z \end{pmatrix} \tag{4}$$

or further as

$$\underbrace{r\mathbf{e}_r}_{\mathbf{u}} := \begin{pmatrix} X \\ Y \\ Z \end{pmatrix} \tag{5}$$

Here,

$$r = \sqrt{X^2 + Y^2 + Z^2} \tag{6}$$

is the radial distance between a surface point of interest $(X, Y, Z)^\top$ and the source of light located at the center of the spherical coordinate system. Moreover, $\mathbf{e}_r$ represents the element of the orthonormal basis vectors in a spherical coordinate system and in direction of the radial depth coordinate $r$. One could further write $\mathbf{e}_r$ as

$$\mathbf{e}_r = \frac{(X, Y, Z)^T}{\sqrt{X^2 + Y^2 + Z^2}} \tag{7}$$

Let us now make explicit how to convert the Cartesian coordinates shown in (4) using trigonometric expressions to spherical ones, i.e.

$$\mathbf{u} = \begin{pmatrix} X \\ Y \\ Z \end{pmatrix} = \begin{pmatrix} r\sin\theta\cos\phi \\ r\sin\theta\sin\phi \\ r\cos\theta \end{pmatrix} \tag{8}$$

Here, one may obtain

$$\theta = \arccos \frac{Z}{\sqrt{X^2 + Y^2 + Z^2}} \tag{9}$$

and

$$\phi = \begin{cases} \arctan(y/x), & x > 0 \\ \arctan(y/x) + \pi, & x < 0 \wedge y \geq 0 \\ \arctan(y/x) - \pi, & x < 0 \wedge y < 0 \\ +\pi/2, & x = 0 \wedge y > 0 \\ -\pi/2, & x = 0 \wedge y < 0 \\ \text{undefined}, & x = 0 \wedge y = 0 \end{cases} \tag{10}$$

### B. Gradient in Spherical Coordinates

We observe that (6), (9) and (10) display the dependency of $r$, $\theta$ and $\phi$ on the Cartesian coordinates $X$, $Y$ and $Z$. This allows us to employ the chain rule and write the differential operators $\partial/\partial r$, $\partial/\partial \theta$ and $\partial/\partial \phi$ based on the differential operators $\partial/\partial X$, $\partial/\partial Y$ and $\partial/\partial Z$:

$$\frac{\partial}{\partial r} = \frac{\partial}{\partial X}\frac{\partial X}{\partial r} + \frac{\partial}{\partial Y}\frac{\partial Y}{\partial r} + \frac{\partial}{\partial Z}\frac{\partial Z}{\partial r} \tag{11}$$

$$\frac{\partial}{\partial \theta} = \frac{\partial}{\partial X}\frac{\partial X}{\partial \theta} + \frac{\partial}{\partial Y}\frac{\partial Y}{\partial \theta} + \frac{\partial}{\partial Z}\frac{\partial Z}{\partial \theta} \tag{12}$$

$$\frac{\partial}{\partial \phi} = \frac{\partial}{\partial X}\frac{\partial X}{\partial \phi} + \frac{\partial}{\partial Y}\frac{\partial Y}{\partial \phi} + \frac{\partial}{\partial Z}\frac{\partial Z}{\partial \phi} \tag{13}$$

However, a more compact form of (11), (12) and (13) could be written using matrix multiplication as

$$\begin{pmatrix} \partial/\partial r \\ \partial/\partial \theta \\ \partial/\partial \phi \end{pmatrix} = \begin{pmatrix} \partial X/\partial r & \partial Y/\partial r & \partial Z/\partial r \\ \partial X/\partial \theta & \partial Y/\partial \theta & \partial Z/\partial \theta \\ \partial X/\partial \phi & \partial Y/\partial \phi & \partial Z/\partial \phi \end{pmatrix} \begin{pmatrix} \partial/\partial X \\ \partial/\partial Y \\ \partial/\partial Z \end{pmatrix} \tag{14}$$

Expanding expressions using (8) one may rewrite the right hand side of the latter equation after a few computations as

$$\begin{pmatrix} \sin\theta\cos\phi & \sin\theta\sin\phi & \cos\theta \\ r\cos\theta\cos\phi & r\cos\theta\sin\phi & -r\sin\theta \\ -r\sin\theta\sin\phi & r\sin\theta\cos\phi & 0 \end{pmatrix} \begin{pmatrix} \partial/\partial X \\ \partial/\partial Y \\ \partial/\partial Z \end{pmatrix} \tag{15}$$

To derive the basis vectors $\mathbf{e}_r$, $\mathbf{e}_\theta$ and $\mathbf{e}_\phi$ and consequently the normal vector to the surface point $\mathbf{u}$, we need to invert the appearing matrix, such that we receive an expression for the gradient operator in terms of the spherical coordinates. After some computations one may obtain

$$\begin{pmatrix} \partial/\partial X \\ \partial/\partial Y \\ \partial/\partial Z \end{pmatrix} = \begin{pmatrix} \sin\theta\cos\phi & \frac{\cos\theta\cos\phi}{r} & \frac{-\sin\phi}{r\sin\theta} \\ \sin\theta\sin\phi & \frac{\sin\phi\cos\theta}{r} & \frac{\cos\phi}{r\sin\theta} \\ \cos\theta & \frac{-\sin\theta}{r} & 0 \end{pmatrix} \begin{pmatrix} \partial/\partial r \\ \partial/\partial \theta \\ \partial/\partial \phi \end{pmatrix} \tag{16}$$

as the result.

## C. Basis Vectors in Spherical Coordinates

We proceed by rewriting (16) in a more compact way as

$$\begin{pmatrix} \partial/\partial X \\ \partial/\partial Y \\ \partial/\partial Z \end{pmatrix} = \mathbf{e}_r \left( \partial/\partial r \right) + \frac{1}{r} \mathbf{e}_\theta \left( \partial/\partial \theta \right) + \frac{1}{r \sin \theta} \mathbf{e}_\phi \left( \partial/\partial \phi \right) \quad (17)$$

Here $\mathbf{e}_r$, $\mathbf{e}_\theta$ and $\mathbf{e}_\phi$ are the basis vectors of the spherical coordinate system, and at the same time represents the orthonormal basis of $\mathbb{R}^3$, that are derived by normalizing the columns of the matrix in (16):

$$\mathbf{e}_r = \begin{pmatrix} \sin \theta \cos \phi \\ \sin \theta \sin \phi \\ \cos \theta \end{pmatrix}, \mathbf{e}_\theta = \begin{pmatrix} \cos \theta \cos \phi \\ \cos \theta \sin \phi \\ -\sin \theta \end{pmatrix}, \mathbf{e}_\phi = \begin{pmatrix} -\sin \phi \\ \cos \phi \\ 0 \end{pmatrix}$$
$$(18)$$

By considering the derivatives in (17), we compile the components related to changes observable over the unit sphere as

$$\nabla_{(\theta,\phi)} := \begin{pmatrix} \frac{1}{r \sin \theta} \frac{\partial}{\partial \phi} \\ \frac{1}{r} \frac{\partial}{\partial \theta} \end{pmatrix} \quad (19)$$

With the same approach, we may derive just the $\theta$-part of the normal vector as given in a *polar coordinate system* as

$$\nabla_{(\theta)} := \frac{1}{r} \frac{\partial}{\partial \theta} \quad (20)$$

Note that one may compute $\frac{\partial}{\partial \theta} \mathbf{e}_r$ and $\frac{\partial}{\partial \phi} \mathbf{e}_r$ as

$$\frac{\partial}{\partial \theta} \mathbf{e}_r = \frac{\partial}{\partial \theta} \begin{pmatrix} \sin \theta \cos \phi \\ \sin \theta \sin \phi \\ \cos \theta \end{pmatrix} = \mathbf{e}_\theta \quad (21)$$

and

$$\frac{\partial}{\partial \phi} \mathbf{e}_r = \frac{\partial}{\partial \phi} \begin{pmatrix} \sin \theta \cos \phi \\ \sin \theta \sin \phi \\ \cos \theta \end{pmatrix} = \sin \theta \cdot \mathbf{e}_\phi \quad (22)$$

respectively. These identities will be used for deriving the normal vector to the surface in next subsection.

## D. Surface Normals in Spherical Setting

By knowing, $\mathbf{e}_r$, $\mathbf{e}_\theta$ and $\mathbf{e}_\phi$ to establish a right-handed coordinate system, the cross product $\frac{\partial \mathbf{u}}{\partial \phi} \times \frac{\partial \mathbf{u}}{\partial \theta}$ will give us a normal vector. Below we sketch the computation:

$$\mathbf{n} \overset{(4)}{=} \frac{\partial \mathbf{u}}{\partial \phi} \times \frac{\partial \mathbf{u}}{\partial \theta} = \frac{\partial (r \mathbf{e}_r)}{\partial \phi} \times \frac{\partial (r \mathbf{e}_r)}{\partial \theta}$$

$$= r \frac{\partial r}{\partial \phi} (\mathbf{e}_r \times \mathbf{e}_\theta) + r \frac{\partial r}{\partial \theta} (\sin \theta \mathbf{e}_\phi \times \mathbf{e}_r) + r^2 (\sin \theta \mathbf{e}_\phi \times \mathbf{e}_\theta)$$

$$= r \frac{\partial r}{\partial \phi} (\mathbf{e}_\phi) + r \sin \theta \frac{\partial r}{\partial \theta} (\mathbf{e}_\phi \times \mathbf{e}_r) + r^2 \sin \theta (\mathbf{e}_\phi \times \mathbf{e}_\theta)$$

$$= r \frac{\partial r}{\partial \phi} \mathbf{e}_\phi + r \sin \theta \frac{\partial r}{\partial \theta} \mathbf{e}_\theta - r^2 \sin \theta \mathbf{e}_r$$

Thus one could write the normal vector $\mathbf{n}$ as

$$\mathbf{n} = \begin{pmatrix} r \frac{\partial r}{\partial \phi} \\ r \sin \theta \frac{\partial r}{\partial \theta} \\ -r^2 \sin \theta \end{pmatrix} \quad (23)$$

that realises itself with respect to the basis vectors $\left( \mathbf{e}_r, \mathbf{e}_\theta, \mathbf{e}_\phi \right)^\top$. The Euclidean norm of $\mathbf{n}$ can be computed as

$$\|\mathbf{n}\| = r \sqrt{ \left( \frac{\partial r}{\partial \phi} \right)^2 + \sin^2 \theta \left( \frac{\partial r}{\partial \theta} \right)^2 + r^2 \sin^2 \theta } \quad (24)$$

## E. Illumination

As we desire to put the source of light located at the center of the spherical coordinate system, we are in a spherical coordinate system in the position to write it in a very simple format, namely

$$\omega = (0, 0, -1)^T \quad (25)$$

Such a light vector has two major properties, *(i)* it always points to the center of the spherical coordinate system, and *(ii)* the inward normal vectors to any surface parametrized in the spherical coordinate system has the same direction with $\omega$.

## F. The PDE of spherical PSFS

We now put the developments together to formulate the brightness equation (26) of PSFS with no light attenuation term in spherical coordinates. We have by Lambert's law

$$I = \rho \left( \omega \cdot \frac{\mathbf{n}}{\|\mathbf{n}\|} \right) \overset{\rho=1}{\iff} I \|\mathbf{n}\| = \omega \cdot \mathbf{n} \quad (26)$$

We recall that $I$ and $\omega$ are the image irradiance of the input image and the light vector, respectively. Substituting the computed expressions (23) and (25) in (26), we obtain

$$\omega \cdot \mathbf{n} = (0, 0, -1)^\top \cdot \begin{pmatrix} r \frac{\partial r}{\partial \phi} \\ r \sin \theta \frac{\partial r}{\partial \theta} \\ -r^2 \sin \theta \end{pmatrix} = r^2 \sin \theta \quad (27)$$

By substituting (19), (24) and (27) in (26), we come after a few more steps of computation to the *eikonal PDE in spherical coordinates*

$$\left\| \nabla_{(\theta,\phi)} u(\phi, \theta) \right\| = \sqrt{ \frac{1}{I(\phi,\theta)^2} - 1 } \quad (28)$$

In coming sections, we prefer to work with one dimension lower than possible, i.e. inside a polar coordinate system which can easily be extended to the spherical one. We believe that this will help us to explain the way the in which the fast marching [15] is adopted and also to visualise our results more effectively. In polar system our eikonal equation (28) shows as

$$\left\| \nabla_{(\theta)} u(\theta) \right\| = \sqrt{ \frac{1}{I(\theta)^2} - 1 } \quad (29)$$

with $\nabla_{(\theta)}$ defined as (20).

Let us briefly comment on the role of free parameters concerning the depth. As we head for drawing a parallel to the classic orthographic setting in orthographic SFS, one may think that it should be possible to have a free additive parameter w.r.t. the depth as in the orthographic SFS setting.

This may be realised by adding here a constant value $\eta$ to the depth $r$ in a polar system as

$$\hat{r} = r + \eta \tag{30}$$

However, as (20) shows, the depth parameter is part of the differential operators in a polar or spherical system. Writing

$$\nabla_{(\theta)} := \frac{\beta}{r+\eta} \frac{\partial}{\partial \theta} \tag{31}$$

setting

$$\beta := {(r+\eta)}/{r} \tag{32}$$

we see that a multiplicative parameter $\beta$ can be chosen to compensate a shift $\eta$ occurred for a curve as the result of its $r$ coordinate change inside a polar system. A simple, additive shift in the $r$ coordinate is not an invariant in this formulation.

## IV. SOLVING SPHERICAL EIKONAL PDE

To solve the eikonal equation (29) we adopt a solution vector $U$ such that

$$U_j := j \cdot h_\theta \tag{33}$$

having

- $j \in \mathbb{N}$ acting as an index,
- $h_\theta$ is a fixed step size, representing the distance among any pair of adjacent cells in our vector $U$.

We start by taking the operator in (20) and replace its $1/r$ term by $1/u$, so that

$$\nabla_{(\theta)} u(\theta) := \frac{1}{u(\theta)} \frac{\partial u(\theta)}{\partial \theta} \tag{34}$$

Now, we replace $\nabla_{(\theta)} u$ appeared in (29) with its discretised backward/forward approximations as

$$\sqrt{\left(\frac{1}{U_{j-1}} \cdot \frac{U_{j-1} - U_j}{h_\theta}\right)^2} = \sqrt{\frac{1}{I^2(\theta_j)} - 1} \tag{35}$$

respectively

$$\sqrt{\left(\frac{1}{U_{j+1}} \cdot \frac{U_{j+1} - U_j}{h_\theta}\right)^2} = \sqrt{\frac{1}{I^2(\theta_j)} - 1} \tag{36}$$

We will make use of these discrete forms in the fast marching method.

Here, $h_\theta$, $I(\theta_j)$ and $U_j$ are all known, whereas both $U_{j-1}$ and $U_{j+1}$ are unknowns. Here onward, we take steps towards rewriting (35) and (36) so that they are numerically solveable in form of a *fixed point iteration* approach. We briefly demonstrate the procedure at hand of (35). To start, we introduce the *new* and the *old* instances of $U_{j-1}$

$$\frac{1}{U_{j-1}^{old}} \cdot \frac{U_{j-1}^{new} - U_j}{h_\theta} = \sqrt{\frac{1}{I^2(\theta_j)} - 1} \tag{37}$$

One may notice that in the context of the fast marching method we employ, in (37) we always have

$$\frac{U_{j-1}^{new} - U_j}{h_\theta} \geq 0 \tag{38}$$

and the data $U_{j-1}^{old}$ is known.

For initialization of the above iteration, we set the unknown term $U_{j-1}^{old}$ inside (37) using its already known neighbor $U_j$.

Now, we take the only unknowns in (37), namely $U_{j-1}^{new}$ to one side that leads to

$$U_{j-1}^{new} = U_j + h_\theta \cdot U_{j-1}^{old} \sqrt{\frac{1}{I^2(\theta_j)} - 1} \tag{39}$$

To solve the eikonal PDE (29), we find the fixed point at each point $j$ iteratively. More precisely, we start by taking (39) and keep on recursively updating $U_{j-1}^{new}$ based on $U_j$ and $U_{j-1}^{old}$ until $\left| U_{j-1}^{new} - U_{j-1}^{old} \right| < \varepsilon$. At that point we adopt $U_{j-1} := U_{j-1}^{new}$ and proceed at node $j-2$.

The analogous procedure can be performed for the forward discretization in the other direction.

## V. EXAMPLE FOR CONVEX-CONCAVE AMBIGUITY

We start the discussion by taking the irradiance signal shown in Figure 3 which is produced based on the black curve shown in Figure 4, which we denote here as *concave curve* in analogy to the orthographic setting. Let us stress that the concave curve takes on the role of the given geometry. Note that, the irradiance signal at the point $(1, {3\pi}/{2})$ is drawn as a bullet. The reason behind is our original concave curve visualised as black inside the Figure 4 does not have a well defined gradient at the point $(6.5, {3\pi}/{2})$. Such bullet is observed in all coming irradiance signals created based on the concave curve.
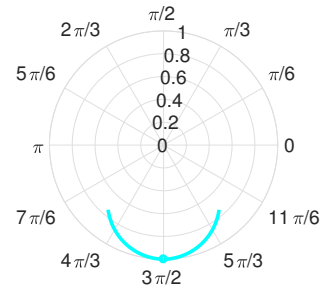
Fig. 3: The input irradiance signal corresponding to the concave curve – with the shape of a hat function – shown in Figure 4, depicted there in black. The bullet mentions that our original concave curve visualised as black inside the Figure 4 does not have a well defined gradient at the point $(6.5, {3\pi}/{2})$.

We now solve the eikonal equation (29) by providing it the given irradiance signal. This produces a *convex curve* depicted in red in Figure 4.

Let us note that we obtain here computationally a convex curve as we enforce this by the construction of the fast
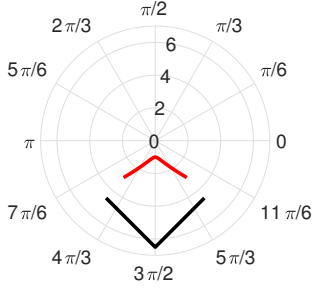
Fig. 4: A pair of concave and convex curves shown as black and red colors, respectively. The former one is the original curve and the latter one is produced by adopting the irradiance signal, shown as Figure 3, and the eikonal equation shown as (29).

marching method, as explained in the previous paragraph. The point in the numerical construction is, that in setting the sign within the square in (35) of the backward/forward differences, we force here the computed solution to have a higher depth value than of one point that must be given to the algorithm for starting. Here, we gave the depth of the top point of the convex curve to the method, leaving the construction of the actual shape to the method.

In order to see that our proceeding has indeed given the sought ambiguity, we now employ another means to verify this by asking if both curves shown in Figure 4 have the same irradiance signals. To perform this test, we adopt (26) in order to compute the irradiance signals taking into account the normal vectors that can be computed for both curves, the result of which is displayed in Figure 5. We observe the desired result, namely that both convex/concave curves shown inside the Figure 4 have effectively the same irradiance signals.
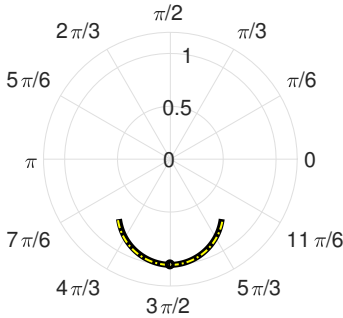


Fig. 5: A nearly indistinguishable pair of irradiance signals shown in solid black and dashed, respectively. The former belongs to the concave curve and the latter corresponds to the convex curve shown in Figure 4.

Finally, let us clarify the impact of the possible free parameters in the new model. We explore this by showing that the convex curve shown in red in Figure 6 can be transformed by keeping the same irradiance signal.

The originally computed solution itself is shown as the red curve in Figure 4, and we see that the top point has the depth

$r = 1$. Thus, adding $\eta = -1$ uniformly to the $r$ coordinates *plus* using the multiplicative change as we elaborated, we produce the transformed convex curve shown in Figure (6).

To make clear that the elaborated combination of additive and multiplicative changes enables to produce an invariant irradiance signal, we perform now exactly this clarification. Once again we produce the irradiance signals of both curves under question and show them as Figure 7. As one observes, both irradiance signals overlap each other with an inaccuracy represented with a hallow bullet around the point $(I = 1, \theta = {}^{3\pi}/2)$. The reason behind the hollow bullet is again that the gradient in polar system (20) is not defined if $r = 0$, that makes the irradiance signal corresponding to the transformed curve undefined. Moreover, the irradiance signal of the concave curve is not also well defined at the mentioned point.
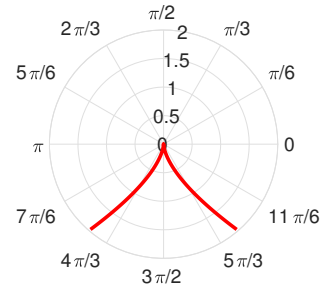


Fig. 6: Our transformed convex curve, produced by adding the value of $\eta = -1$ to the $r$ coordinate of the computed convex curve shown in Figure 4, and adopting the corresponding multiplicative parameter to compensate the effect of the transformation. One could observe that the irradiance signal of the transformed convex curve coincides with the one corresponding to the computed convex curve shown inside the Figure 7.
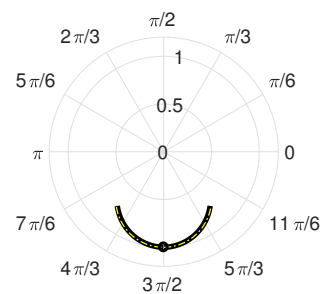


Fig. 7: Comparison of irradiance signals shown as solid black and dashed yellow. The former belongs to the *convex curve* shown in Figure 4 and the latter corresponds to the transformed curve shown inside the Figure 6. The hollow bullet represents the fact that the irradiance values of the curve shown in Figure 6 around the point $(I = 1, \theta = {}^{3\pi}/2)$ is not defined. The curves coincide to a large degree.

## VI. CONCLUSION

We have verified the existence of the convex/concave ambiguity in a perspective SFS model. In our presented example

we have assured that every step is validated with respect to this goal. Our assumption about the light position as well as the decision not to take into account an attenuation term allowed our constituting equation of PSFS to be represented as an eikonal equation of the identical form as in classic, orthographic SFS. The main point in our proceeding was thereby the use of the spherical coordinate system. It is evident that the described proceeding for the construction of the ambiguity can easily be performed in the full spherical system i.e. for images instead of signals. In future work we will extend the considerations about ambiguities and work on ways to resolve them.

## REFERENCES

[1] M. Breuß, E. Cristiani, J.-D. Durou, M. Falcone, and O. Vogel, Perspective Shape from Shading: Ambiguity Analysis and Numerical Approximations. SIAM Journal on Imaging Sciences, 5 (2012), 1, 311–342.

[2] A.R. Bruss, The eikonal equation: some results applicable to computer vision. Journal of Mathematical Physics, 23 (1982), 890–896.

[3] F. Courteille, A. Crouzil, J.-D Durou, and P. Gurdjos: Towards shape from shading under realistic photographic conditions. In Proc. ICPR, 2004, 277–280.

[4] S. Galliani, Y.C. Ju, M. Breuß and A. Bruhn: Generalised Perspective Shape from Shading in Spherical Coordinates. In Proc. SSVM, 2013, 222–233.

[5] B.K.P. Horn, Shape from Shading: A Method for Obtaining the Shape of a Smooth Opaque Object from One View. PhD thesis, Department of Electrical Engineering, MIT, Cambridge, Massachusetts, USA, 1970.

[6] B.K.P. Horn, Robot Vision. MIT Press, 1986.

[7] B.K.P. Horn and M.J. Brooks, Shape from Shading. Artificial Intelligence Series, MIT Press, 1989.

[8] Y.C. Ju, S. Tozza, M. Breuß, A. Bruhn and A. Kleefeld, Generalised Perspective Shape from Shading with Oren-Nayar Reflectance. In Proc. BMVC, 2013, Article 42.

[9] J.J. Koenderink, What does the occluding contour tell us about solid shape? Perception, 13(3):321330, 1984.

[10] K.M. Lee and C.C.J. Kuo, Shape from Shading with Perspective Projection. Computer Vision, Graphics, Image Processing: Image Understanding 59, No. 2 (1994), 202–211.

[11] B. Liu and J.T. Todd, Perceptual biases in the interpretation of 3d shape from shading. Vision research, 44(18):21352145, 2004.

[12] E. Prados and O. Faugeras, Perspective Shape from Shading and Viscosity Solutions. In Proc. ICCV, 2003, vol. II, 826–831.

[13] E. Prados, F. Camilli, and O. Faugeras, A unifying and rigorous shape from shading method adapted to realistic data and applications. J. Math. Imag. and Vis. 25 (2006), 3, 307–328.

[14] E. Prados, F. Camilli, and O. Faugeras: A viscosity solution method for shape-from-shading without image boundary data. M2AN Math. Model. Numer. Anal. 40 (2006), 2, 393–412.

[15] J.A. Sethian, Level set methods and fast marching methods: evolving interfaces in computational geometry, fluid mechanics, computer vision, and materials science. Cambridge University Press, 1999.

[16] A. Tankus, N. Sochen, and Y. Yeshurun, A New Perspective [on] Shape-from-Shading. In: Proc. 9th IEEE Int. Conf. Comp. Vis. (vol. II), Nice, France, October 2003, pp. 862–869.

[17] R. Zhang, P.S. Tsai, J.E. Cryer, and M. Shah, Shape-from-shading: a survey. IEEE Trans. Pattern Anal. Mach. Intell., 21 (1999), 690–706.